PNAS RESEARCH ARTICLE | CHEMISTRY

Ring-opening metathesis polymerization of *N*-methylpyridinium-fused norbornenes to access antibacterial main-chain cationic polymers

Sarah N. Hancock[a], Nattawut Yuntawattana[a,1,2], Emily Diep[b,1], Arunava Maity[a], An Tran[a], Jessica D. Schiffman[b,3], and Quentin Michaudel[a,c,3]

Edited by Craig Hawker, University of California Santa Barbara, Santa Barbara, CA; received July 5, 2023; accepted October 31, 2023

Cationic polymers have been identified as a promising type of antibacterial molecules, whose bioactivity can be tuned through structural modulation. Recent studies suggest that the placement of the cationic groups close to the core of the polymeric architecture rather than on appended side chains might improve both their bioactivity and selectivity for bacterial cells over mammalian cells. However, antibacterial main-chain cationic polymers are typically synthesized via polycondensations, which do not afford precise and uniform molecular design. Therefore, accessing main-chain cationic polymers with high degrees of molecular tunability hinges upon the development of controlled polymerizations tolerating cationic motifs (or cation progenitors) near the propagating species. Herein, we report the synthesis and ring-opening metathesis polymerization (ROMP) of *N*-methylpyridinium-fused norbornene monomers. The identification of reaction conditions leading to a well-controlled ROMP enabled structural diversification of the main-chain cationic polymers and a study of their bioactivity. This family of polyelectrolytes was found to be active against both Gram-negative (*Escherichia coli*) and Gram-positive (Methicillin-resistant *Staphylococcus aureus*) bacteria with minimal inhibitory concentrations as low as 25 μg/mL. Additionally, the molar mass of the polymers was found to impact their hemolytic activity with cationic polymers of smaller degrees of polymerization showing increased selectivity for bacteria over human red blood cells.

ROMP | antibacterial | cationic polymers | controlled polymerization

Antibiotic-resistant bacteria, such as methicillin-resistant *Staphylococcus aureus* (MRSA), are a rapidly growing threat to public health (1). Without the identification of new antibiotics, common injuries and minor infections may once again prove lethal (2, 3). Synthetic cationic polymers have emerged as an effective class of antibacterial agents (4–9). Unlike antibiotics that target intercellular functions, cationic polymers primarily interact with the surface of the lipid membranes of Gram-negative and Gram-positive bacteria, which leads to physical damage to the cell (4, 10–12). This unique mechanism has been shown to be less likely to induce antibiotic resistance (13). While the precise relationships between bactericidal activity and polymer architecture remain unclear (4–9), a careful balance of cationic and hydrophobic motifs is required. Similar to host defense peptides (14), cationic groups allow electrostatic interactions with the negatively charged membranes of bacteria while hydrophobic segments facilitate insertion and disruption of the membranes (4, 5, 9). To this end, the location of the cationic group vis-à-vis the main chain has been identified as a key parameter (5, 9).

Cationic heads are often located on the side chains to facilitate monomer synthesis and polymerization. For example, several examples of monomers for reversible-deactivation radical polymerization (RDRP) or ring-opening metathesis polymerization (ROMP) have been synthesized with cations or cation progenitors distal to the reactive alkene group (15–26). Of note, cations are often introduced in a postpolymerization step through deprotection followed by protonation or alkylation of a Lewis basic site (15, 16, 18–22, 24, 25). These monomers have permitted the precise preparation of polymers containing various cationic motifs separated from the backbone and the investigation of their bioactivity (Fig. 1*A*). Interestingly, a recent study by Mao and Yan directly compared the activity between main-chain cationic placement vs. that of a side chain; the former exhibited a drastically improved antibacterial activity as well as a lower hemolytic activity, both of which are crucial for therapeutic applications (Fig. 1*B*) (27). A similar finding was reported by Perrier and coworkers with star polymers, which exhibited lower levels of undesired aggregation of red blood cells when cation motifs were shifted from the arms to the core (28). Finally, Noonan and Palermo demonstrated that shorter cationic side chains that placed the charges closer to the backbone led to faster bactericidal kinetics (26). While placing cations along the polymer backbone represents a promising structural design, this strategy also provides an

Significance

The rapid emergence of antibiotic-resistant bacteria has been identified as a global threat by the World Health Organization, which has called for the urgent development of novel antibiotics. Cationic polymers are a promising class of bioactive agents, which trigger bacterial cell death through physical disruption of their membranes. However, polymerization processes must be designed to optimize the therapeutic potential of cationic polymers. In this work, we report the precise synthesis of main-chain cationic polymers via controlled ring-opening metathesis polymerization of *N*-methylpyridinium-fused norbornenes. These charged polymers were found to be active against both Gram-positive and -negative bacteria. Additionally, modification of the chain length and pyridinium core allowed for the improvement of their selectivity for bacterial cells over human red blood cells.

The authors declare no competing interest.

This article is a PNAS Direct Submission.

[1]N.Y. and E.D. contributed equally to this work.

[2]Present address: Department of Materials Science, Faculty of Science, Kasetsart University, Bangkok 10900, Thailand.

[3]To whom correspondence may be addressed. Email: schiffman@umass.edu or quentin.michaudel@chem.tamu.edu.

This article contains supporting information online at https://www.pnas.org/lookup/suppl/doi:10.1073/pnas.2311396120/-/DCSupplemental.

Published December 11, 2023.

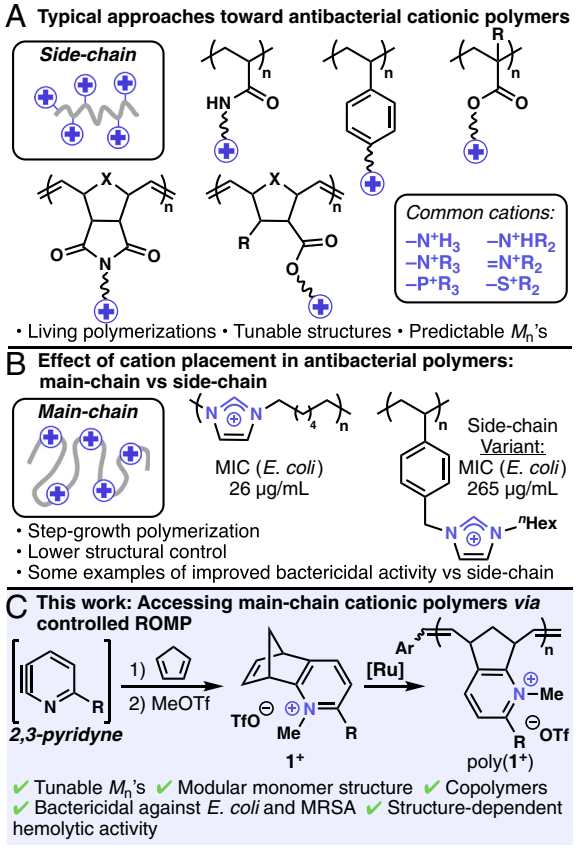

Fig. 1. (*A*) Examples of side-chain cationic polymer backbones afforded through controlled polymerization. (*B*) Cation placement on backbone increases bactericidal activity; MIC: minimal inhibitory concentration. (*C*) ROMP of *N*-methylpyridinium-fused norbornene monomers.

exciting synthetic challenge: Installation of main-chain cation components in antibacterial macromolecules has thus far mostly been achieved through polycondensations (27, 29–42), which limits modulation of the polymer architecture. The development of suitable monomers for the precise synthesis of main-chain cationic

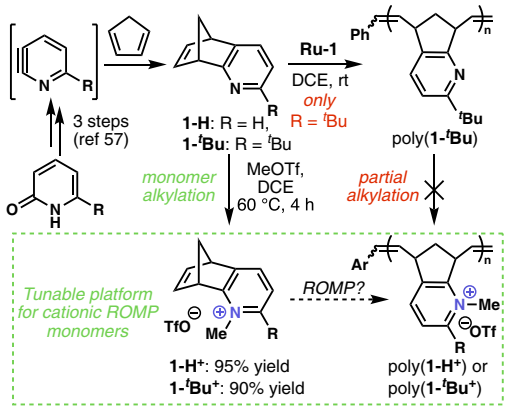

Fig. 2. Different routes toward main-chain cationic polymers: postpolymerization alkylation of poly(**1-^{t}Bu**) vs. synthesis of cationic ROMP monomers **1-H$^+$** and **1-^{t}Bu$^+$**.

polymers would therefore permit exhaustive structure–activity relationship studies through the variation of structural parameters including comonomer composition and molar mass distribution, which impact antibacterial activity (43–48). Additionally, the ability to manufacture nanomaterials with a narrow size distribution is considered a critical quality attribute by the US Food and Drug Administration to ensure batch-to-batch reproducibility (49). Last but not least, the development of the precise syntheses of cationic polymers represents an opportunity to identify materials for other disruptive technologies. For example, the search of alkaline-stable anion exchange membranes for fuel cells has driven the design of a variety of cationic polymers (50–56), including cation-functionalized polyethylene copolymers prepared via ROMP of imidazolium-fused *trans*-cyclooctene derivatives (53, 54).

Herein, we report the ROMP of two pyridinium-fused norbornene monomers synthesized via cycloaddition of cyclopentadiene and pyridyne derivatives followed by nitrogen alkylation (Fig. 1*C*). These monomers were designed to embed the cationic pyridiniums directly onto the polymer main chain rather than onto flexible pendent groups. Optimization of the ROMP process

Table 1. ROMP of 1-H$^+$ and 1-^{t}Bu$^+$ with catalysts Ru-1–3

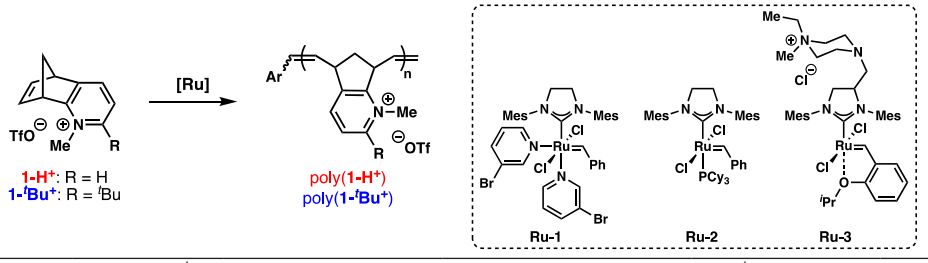

Entry*	1$^+$	Ru	Solvent†	Temperature (°C)	Time (h)	Conv (%)	M_n^{theo} (kg/mol)	M_n^{exp} (kg/mol)†	$Đ$†
1	**1-H$^+$**	**Ru-1**	EtOH/DCM	23	24	13	n.d.	n.d.	n.d.
2	**1-H$^+$**	**Ru-1**	TFE/DCM	23	24	7	n.d.	n.d.	n.d.
3	**1-H$^+$**	**Ru-1**	EtOH/DCM	60	24	47	n.d.	n.d.	n.d.
4	**1-H$^+$**	**Ru-2**	EtOH/DCM	60	5	>99	12.5	24.0	3.00
5	**1-H$^+$**	**Ru-3**	EtOH	60	3.5	>99	12.5	23.5	1.33
6	**1-^{t}Bu$^+$**	**Ru-1**	EtOH/DCM	60	24	40	n.d.	n.d.	n.d.
7	**1-^{t}Bu$^+$**	**Ru-2**	EtOH/DCM	60	5	>99	14.7	15.0	1.62
8	**1-^{t}Bu$^+$**	**Ru-3**	EtOH	60	3.5	>99	14.7	24.1	1.28

*Monomer (**1-H$^+$** or **1-^{t}Bu$^+$**, 65 μmol) was polymerized by **Ru** catalysts (1.6 μmol).
†M_n and $Đ$ values were determined by SEC (TFE eluent) using PMMA standards (RI detection).
EtOH/DCM or TFE/DCM = 10:1. n.d. = not determined.

allowed the synthesis of polymers with living characteristics including predictable molar masses and functionalizable chain ends amenable to the preparation of block copolymers. Notably, postpolymerization functionalization is not required to install the positive charge of the *N*-methylpyridinium subunits, which is also independent of the pH of the media. These main-chain cationic polymers were found to be active against both Gram-negative *Escherichia coli* K12 MG1655 (*E. coli*) and the Gram-positive clinical isolate methicillin-resistant *Staphylococcus aureus* IDRL-6169 (MRSA) bacteria. The effects of molar mass and polymer composition on activity and selectivity were probed and will serve to further optimize the therapeutic index of this family of antibacterial cationic polymers.

Results and Discussion

Synthesis and ROMP of *N*-methylpyridinium-Fused Norbornene Monomers. We recently reported the expedient synthesis of monomers **1-H** and **1-^{t}Bu** from 2,3-pyridyne derivatives. While monomer **1-H** was found to resist productive ROMP potentially because of catalyst poisoning, the more sterically hindered **1-^{t}Bu** underwent successful controlled polymerization using **Ru-1** (57). We hypothesized that neutral poly(**1-^{t}Bu**) could serve as a platform for the preparation of main-chain cationic polymers via alkylation of the repeating pyridine nitrogen. Unfortunately, direct methylation of poly(**1-^{t}Bu**) with highly reactive MeOTf only led to partial alkylation, presumably due to premature precipitation in solvents compatible with the neutral macromolecules including dichloromethane (DCM) and dichloroethane (DCE) (Fig. 2 and *SI Appendix*, Scheme S4). The order of the synthetic sequence was modified to circumvent the challenges of postpolymerization functionalization of poly(**1-^{t}Bu**). This alternative strategy would provide the additional advantage of preventing deleterious coordination from the Lewis basic nitrogen during the ROMP process, thereby allowing the use of nonbulky monomers including derivatives of **1-H**. Methylation of **1-H** and **1-^{t}Bu** with MeOTf was found to proceed in 95 and 90% yield, respectively, to afford cationic monomers **1-H$^+$** and **1-^{t}Bu$^+$** (Fig. 2).

The poor solubility profile of monomers **1-H$^+$** and **1-^{t}Bu$^+$** in polar, aprotic solvents typically used with **Ru-1,2** complicated the identification of suitable ROMP conditions. To achieve a controlled process with high conversions, solvent mixtures were screened (Table 1). Slow polymerization of **1-H$^+$** with **Ru-1** was observed when a (10:1) mixture of ethanol (EtOH) and DCM was used (Table 1, entry 1). Trifluoroethanol (TFE) has been shown to be a suitable solvent for the ROMP of cationic monomers (58); however, this substitution did not facilitate the polymerization of **1-H$^+$** (Table 1, entry 2). Increasing the temperature to 60 °C improved the conversion to 47% after 24 h using **Ru-1** (Table 1, entry 3). When **Ru-2** was used in lieu of **Ru-1**, full conversion of **1-H$^+$** was observed in 5 h (Table 1, entry 4). However, size-exclusion chromatography (SEC) analysis of poly(**1-H$^+$**) using TFE as the eluent revealed a broad molar mass distribution ($Đ$ = 3.00; *SI Appendix*, Fig. S1), which could be the result of undesired chain transfers. To obviate the need of a solvent mixture ensuring catalyst and monomer dissolution, we turned our attention to **Ru-3** (AquaMet), a Hoveyda-Grubbs-type Ru carbene containing an ammonium-functionalized NHC ligand originally developed for ROMP in aqueous media (59). Pleasingly, polymerization of **1-H$^+$** in EtOH at 60 °C with **Ru-3** led to full monomer consumption in 3.5 h, and poly(**1-H$^+$**) was characterized by a molar mass distribution with significantly narrower dispersity ($Đ$ = 1.33; Table 1, entry 5). While the experimental molar mass was found to be higher than the expected value, this can be potentially ascribed to repulsive interactions of the repeating cations causing a larger hydrodynamic radius in TFE relative to the poly (methyl methacrylate) (PMMA) standards (54, 60). Similar discrepancies between experimental and theoretical molar mass (M_n) values have been reported for other ROMP polymers containing polar functional groups (24, 25). Of note, only fluorinated solvent such as TFE or hexafluoroisopropanol were suitable eluents for SEC analysis of these cationic polymers. Interestingly, similar results were observed with the ROMP of **1-^{t}Bu$^+$** despite the presence of a *tert*-butyl substituent rendering the monomer less hydrophilic than **1-H$^+$**. Lower conversion was observed with **Ru-1** compared to **Ru-2** (Table 1, entries 6 and 7), while **Ru-3** provided both >99% conversion and narrow dispersity ($Đ$ = 1.28; Table 1, entry 8). In situ NMR analysis using d_6-EtOD as the solvent revealed a complete initiation of **Ru-3** within 4 min (*SI Appendix*, Fig. S5) suggesting that the rate of initiation (k_i) is high enough relative to the rate of propagation (k_p) to ensure that the degree of polymerization is dictated by the initial feed ratio (61). Careful analysis of ^{1}H and ^{13}C NMR spectra, in combination with COSY, HSQC, and HMBC experiments [*SI Appendix*, Figs. S18–S23 for poly(**1-H$^+$**) and *SI Appendix*, Figs. S24–S29 for poly(**1-^{t}Bu$^+$**)] suggests that these cationic polymers likely exhibit regio irregularities from concurrent head-to-head or head-to-tail pathways. However, *cis*/*trans* olefin stereochemistry and various tacticities could also contribute to the complexity of the NMR spectra.

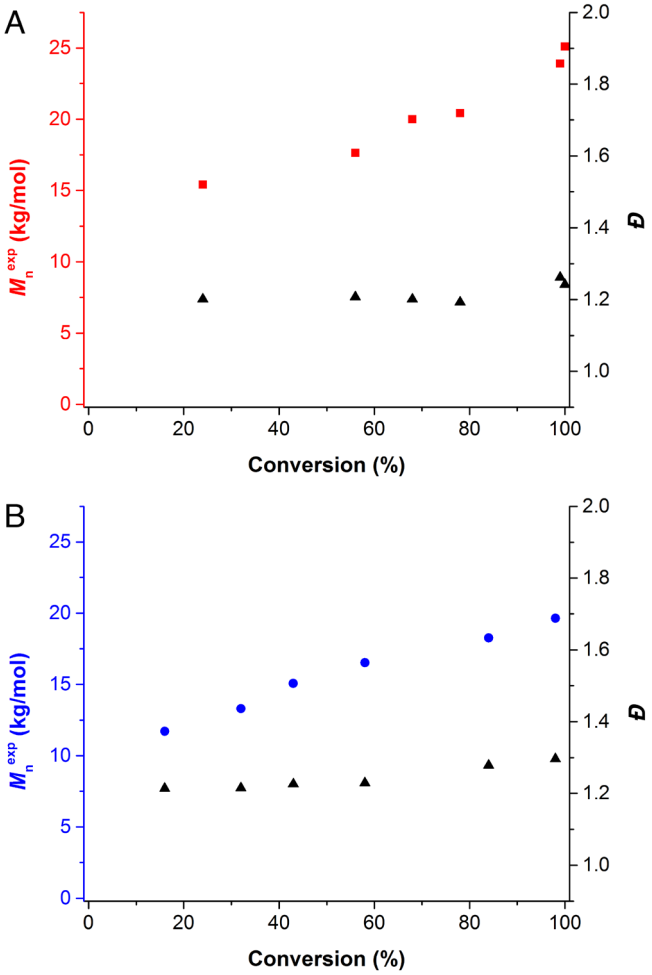

Fig. 3. Polymerization of **1$^+$** with **Ru-3** ([**1$^+$**]:[**Ru-3**] = 40:1): (*A*) M_n^{exp} of poly(**1-H$^+$**) (red squares) and $Đ$ (black triangles) vs. conversion; (*B*) M_n^{exp} of poly(**1-^{t}Bu$^+$**) (blue circles) and $Đ$ (black triangles) vs. conversion.

Thermal Properties of Polymers Poly(1-H$^+$) and Poly(1-^{t}Bu$^+$). In order to gain some insight into the thermal properties of these main-chain cationic polymers, thermogravimetric analysis (TGA) and differential scanning calorimetry (DSC) were performed. Poly(**1**$^+$) was shown to exhibit high thermal stability by TGA with a temperature of decomposition measured at 5% weight loss, T_d = 346 °C for poly(**1**-H$^+$) and T_d = 301 °C for poly(**1**-^{t}Bu$^+$) (*SI Appendix*, Fig. S3). DSC revealed glass transition temperatures (T_g) of 170 °C for poly(**1**-H$^+$) and 183 °C for poly(**1**-^{t}Bu$^+$), which confirmed the stiffness of the backbone of these main-chain cationic polymers (*SI Appendix*, Fig. S4). The rigidity of the main chain likely imparts limited conformational freedom to the fused-pyridinium motifs in contrast to cationic groups appended on polymer side chains (15–26). Crystallization or melting transitions were not observed by DSC for either polymer suggesting a mostly amorphous behavior. Notably, poly(**1**-^{t}Bu$^+$) exhibited T_d and T_g values higher than those of the neutral variant poly(**1**-^{t}Bu) (T_d = 281 °C, T_g = 157 °C) (57).

Investigation of the Kinetics of the ROMP of Monomers 1-H$^+$ and 1-^{t}Bu$^+$. The propagation kinetics were investigated for both **1**-H$^+$ and **1**-^{t}Bu$^+$. Despite the aforementioned overestimation of molar masses measured by SEC, M_n was found to grow linearly with the conversion of both monomers, and dispersity values remained below 1.3 throughout the ROMP (Fig. 3).

While complicated by the polycationic nature of poly(**1**$^+$), MALDI-TOF mass spectrometry of a poly(**1**-^{t}Bu$^+$) 10-mer confirmed a degree of polymerization (DP) close to our target (*SI Appendix*, Fig. S2). Polymers of predictable molar masses were synthesized through the variation of monomer-to-initiator ratios (Fig. 4 *A* and *B*), and the difference between experimental and theoretical M_n values was found to be linear (Fig. 4 *C* and *D*).

To thoroughly characterize the livingness of the polymerization, the rate of propagation of the ROMP of monomers **1**-H$^+$ and **1**-^{t}Bu$^+$ catalyzed by **Ru-3** was studied via ^{1}H NMR in d_4-MeOD. Plotting $\ln([M]_0/[M]_t)$ as a function of time revealed a linear fit and k_p^{app} values of 0.0766 min^{-1} (R^2 = 0.998) and 0.0325 min^{-1} (R^2 = 0.994) for **1**-H$^+$ and **1**-^{t}Bu$^+$, respectively, based on Eqs. **1** and **2**:

$$\frac{-d[M]}{dt} = k_p^{app}[M], \quad [1]$$

$$k_p^{app} = k_p[C], \quad [2]$$

where [M] is the concentration of **1**$^+$ at time t, k_p^{app} the apparent propagation rate constant, k_p the propagation rate constant, and [C] the concentration of **Ru-3** at time t. The measured linear relation between $\ln([M]_0/[M]_t)$ and time confirmed the first-order dependence in concentration of **1**-H$^+$ and **1**-^{t}Bu$^+$, as expected for a living chain-growth process (Fig. 5 *A* and *B*).

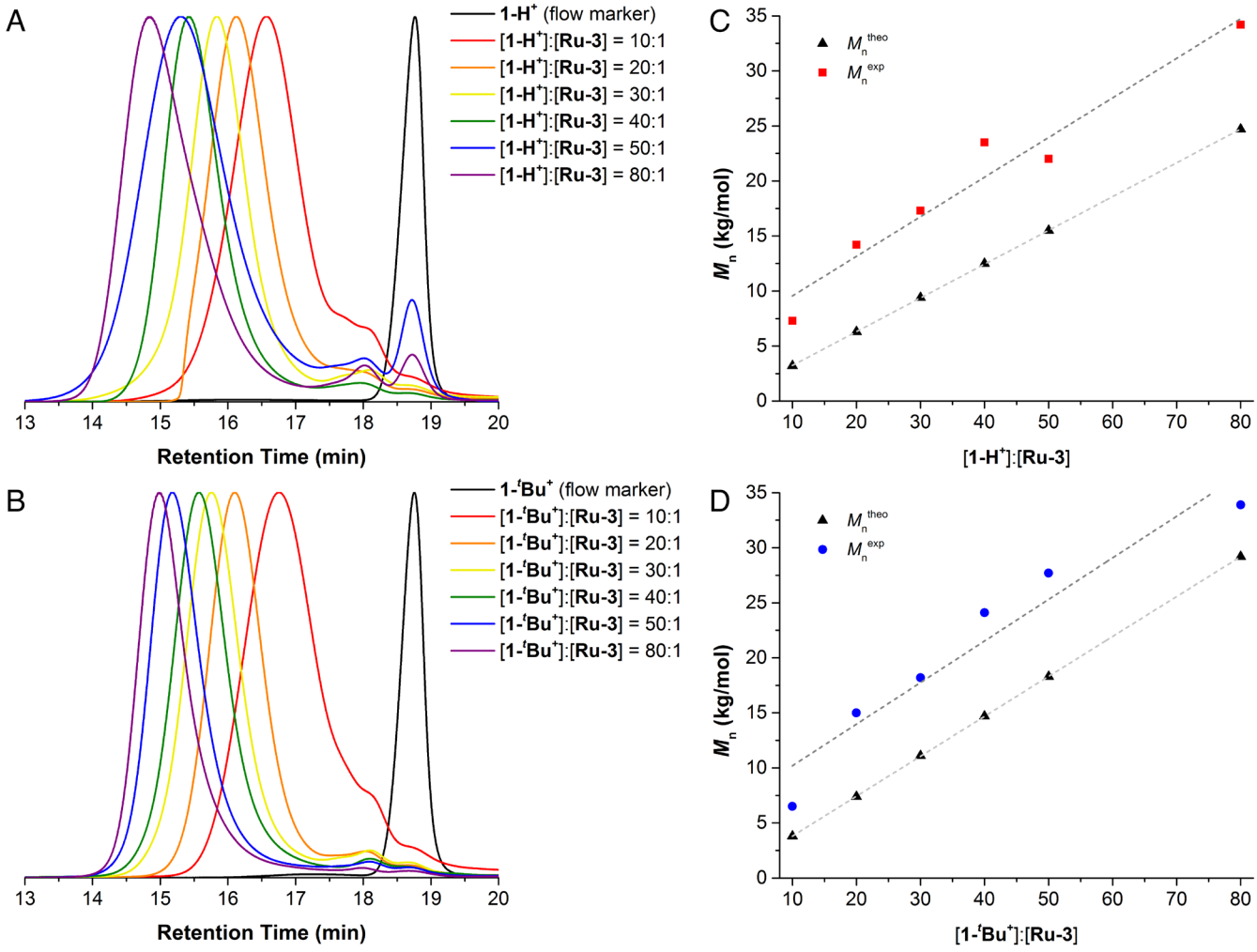

Fig. 4. SEC traces of different DPs of (*A*) poly(**1**-H$^+$) and (*B*) poly(**1**-^{t}Bu$^+$). Dependence of the M_n of (*C*) poly(**1**-H$^+$) on the [**1**-H$^+$]:[**Ru-3**] ratio and (*D*) poly(**1**-^{t}Bu$^+$) on the [**1**-^{t}Bu$^+$]:[**Ru-3**] ratio.

Synthesis of Random and Block Copolymers with Monomers 1-H^+ and 1-^{t}Bu$^+$. The livingness of the optimized ROMP process was confirmed through chain extension of poly(**1**-^{t}**Bu**$^+$) with **1**-H^+ (ratio of **1**-^{t}**Bu**$^+$:**1**-H^+:**Ru-3** = 10:10:1), which provided evidence that the propagating chain ends are preserved after monomer depletion. Full conversion of the second monomer, **1**-H^+, was observed by ^{1}H NMR alongside a shift of the SEC trace corresponding to the following polymers (*SI Appendix*, Fig. S6): For poly(**1**-^{t}**Bu**$^+$), M_n = 9.2 kg/mol, $Đ$ = 1.20 and for poly(**1**-^{t}**Bu**$^+$)-*b*-(**1**-H^+), M_n = 11.0 kg/mol, $Đ$ = 1.33. A single diffusion coefficient observed by DOSY NMR (*SI Appendix*, Fig. S33) confirmed the efficient chain extension of poly(**1**-^{t}**Bu**$^+$). This strategy allowed us to prepare block copolymer poly(**1**-^{t}**Bu**$^+$)-*b*-(**1**-H^+) with two segments of differing hydrophobicity and steric bulk around the cationic group.

To probe the importance of sequence of the repeating cations, a random copolymer was also targeted. Copolymerization of **1**-H^+ and **1**-^{t}**Bu**$^+$ yielded poly(**1**-H^+)-*r*-(**1**-^{t}**Bu**$^+$) (M_n = 11.4 kg/mol, $Đ$ = 1.37). A simultaneous and almost quantitative incorporation of both monomers was observed over 3.5 h via ^{1}H NMR at 60 °C in d_6-EtOD (*SI Appendix*, Fig. S8 and Table S2), while the molar mass distribution of the resulting random copolymer remained narrow and monomodal (*SI Appendix*, Fig. S7).

Antibacterial Susceptibility with Homopolymers Determined by Disk Diffusion Assays. The first investigations into the antibacterial activity of poly(**1**-H^+) and poly(**1**-^{t}**Bu**$^+$) with a DP of 20 were conducted using disk diffusion assays. This method provides a rapid assessment for antibacterial susceptibility rather than a quantitative determination of a minimal inhibitory concentration (MIC) (62–64). Gram-negative *E. coli* K12 and Gram-positive MRSA were selected as laboratory-standard and clinically relevant strains (respectively) to assess the antibacterial activity of poly(**1**$^+$). Disk diffusion assays were conducted by pipetting dilutions of cationic polymers onto filter disks that were incubated on bacteria-inoculated agar plates. While both monomers and poly(**1**-H^+) were found to be soluble in water, poly(**1**-^{t}**Bu**$^+$) and copolymers poly(**1**-^{t}**Bu**$^+$)-*b*-(**1**-H^+) and poly(**1**-H^+)-*r*-(**1**-^{t}**Bu**$^+$) were not and required the use of a polar organic cosolvent. Dimethyl sulfoxide (DMSO) was selected for this study because of its low toxicity to cells, in contrast to most organic solvents (65), and its successful use in prior disk diffusion assays for antibacterial susceptibility testing (66). In parallel to testing the cationic polymers, a control disk, that was only exposed to the relevant solvent used (i.e., water or DMSO without polymers) was also tested.

Poly(**1**-H^+)$_{20}$ dissolved in water showed antibacterial activity as a zone of inhibition (ZOI) at a concentration of 1,600 μg/mL for both bacteria as indicated by yellow arrows in Fig. 6*A*. When DMSO was used to dissolve poly(**1**-H^+)$_{20}$, the concentration needed to inhibit growth of *E. coli* was similar to that of the aqueous solution, while the lowest concentration with a ZOI for MRSA was 800 μg/mL (Fig. 6*B*). Notably, control disks (containing water or DMSO) exhibited no ZOI. The difference in inhibitory concentrations for poly(**1**-H^+)$_{20}$ dissolved in water and in DMSO may be caused by the differences in the diffusion of the cationic polymer and solvent along the hydrophilic agar plate. Meanwhile, *tert*-butyl substituted poly(**1**-^{t}**Bu**$^+$)$_{20}$ dissolved in DMSO exhibited a ZOI at a concentration of 1,600 μg/mL against *E. coli*, and 400 μg/mL against MRSA (Fig. 6*C*). Of note, monomers **1**-H^+ and **1**-^{t}**Bu**$^+$ did not exhibit inhibitory activity against either bacterium at the concentrations screened for disk diffusion assays (*SI Appendix*, Fig. S10 *A–D*). These results indicate the importance of the polycationic structure for antibacterial activity.

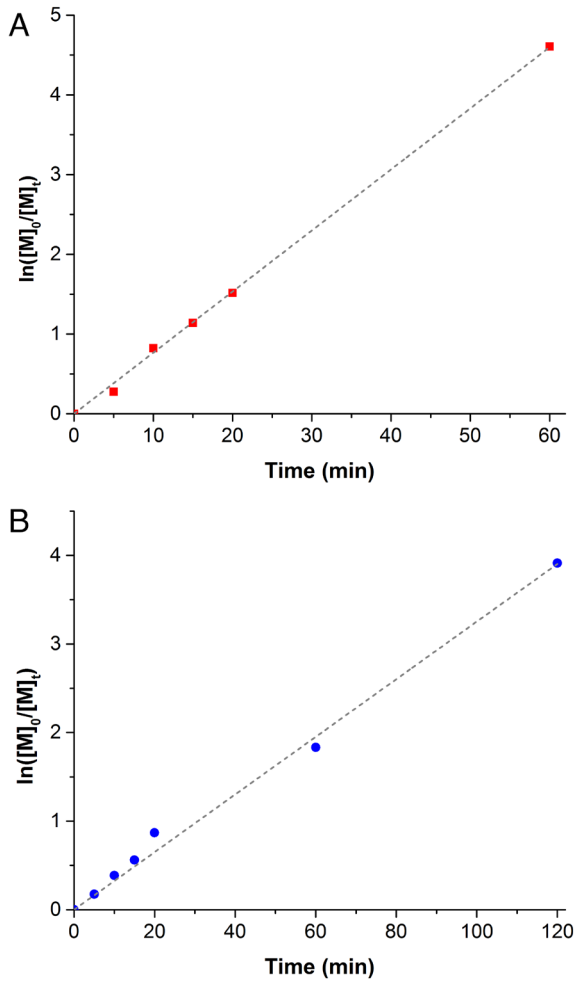

Fig. 5. Determination of the rate of propagation of (*A*) **1**-H^+ (k_p^{app} = 0.0766 min^{-1}, R^2 = 0.998) and (*B*) **1**-^{t}**Bu**$^+$ (k_p^{app} = 0.0325 min^{-1}, R^2 = 0.994).

Antibacterial Susceptibility with Copolymers Determined by Disk Diffusion Assays. The antibacterial activity of block and random copolymers, poly(**1**-^{t}**Bu**$^+$)$_{10}$-*b*-(**1**-H^+)$_{10}$ and poly(**1**-H^+)$_{10}$-*r*-(**1**-^{t}**Bu**$^+$)$_{10}$, respectively, was determined to explore the effect of varying the steric bulk and hydrophobicity surrounding the pyridinium group. Block copolymer poly(**1**-^{t}**Bu**$^+$)$_{10}$-*b*-(**1**-H^+)$_{10}$ showed ZOIs at 3,200 μg/mL for both bacteria (Fig. 6*D*), while random copolymer poly(**1**-H^+)$_{10}$-*r*-(**1**-^{t}**Bu**$^+$)$_{10}$ exhibited MIC values of 6,400 and 3,200 μg/mL for *E. coli* and MRSA, respectively (Fig. 6*E*). The difference in lowest concentrations necessary for a ZOI against *E. coli* between the copolymers suggests that the spatial arrangement of repeating units bearing hydrophobic groups nearby the pyridinium is important to the bactericidal activity of the macromolecules.

MIC Determination by Broth Microdilution Assays. Since the disk diffusion assays suggested that both poly(**1**-H^+) and poly(**1**-^{t}**Bu**$^+$) exhibited antibacterial activity against *E. coli* and MRSA, broth microdilution assays were conducted to determine the MIC values of these polymers. This method provides quantitative MICs since the disk diffusion assay cannot quantify the amount of the antibacterial agent that diffuses along the agar surface (63). In addition to investigating the effect of chemical structure on the antibacterial activity of poly(**1**-H^+) and (**1**-^{t}**Bu**$^+$), the influence of the length of the polymers was also studied. While beyond the scope of this study to identify the exact mechanism

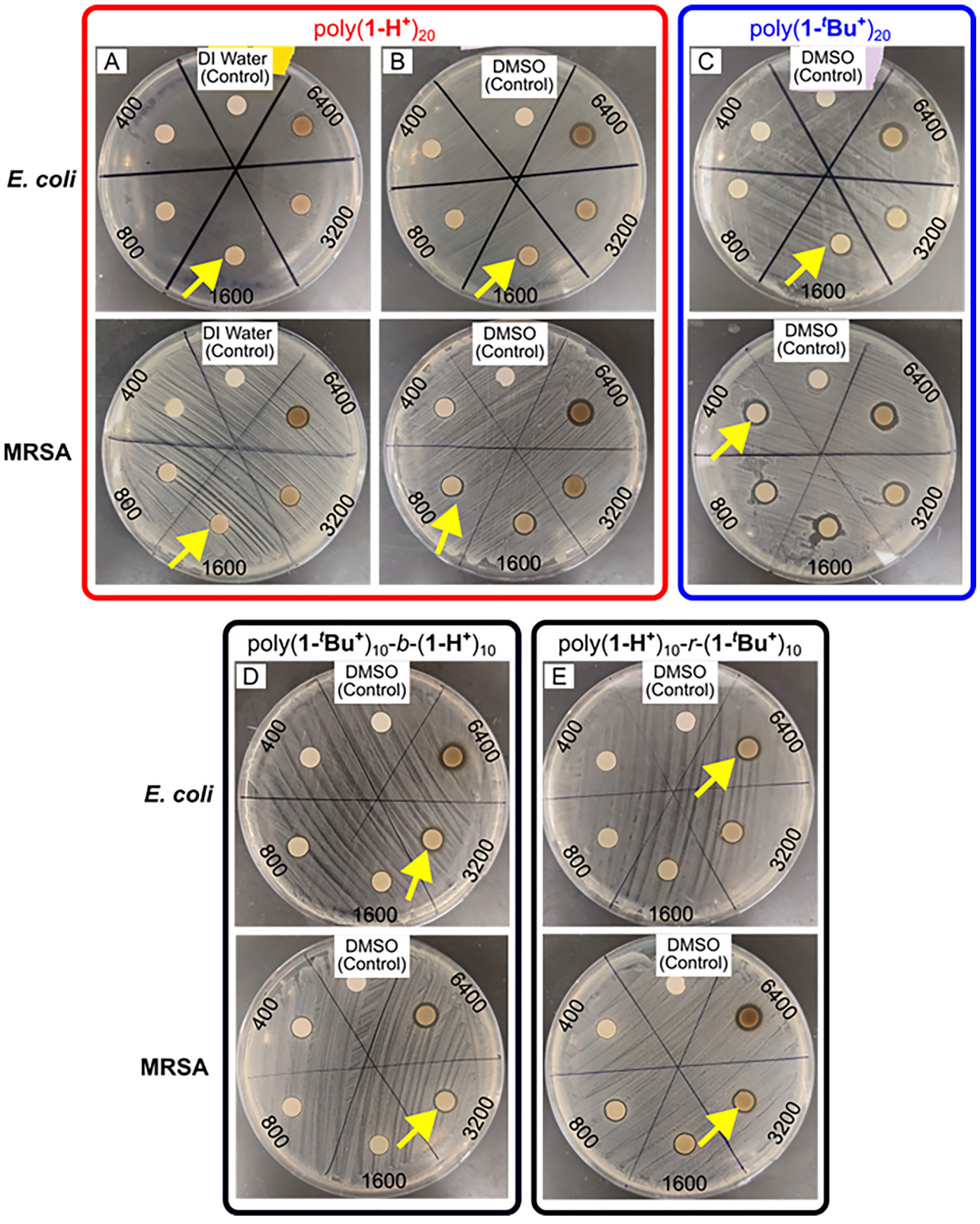

Fig. 6. Disk diffusion assays against *E. coli* and MRSA (with yellow arrows indicating lowest concentration in which a ZOI is observed) for (*A*) poly(**1-H**$^+$)$_{20}$ dissolved in water, (*B*) poly(**1-H**$^+$)$_{20}$ dissolved in DMSO, (*C*) poly(**1-**^{t}**Bu**$^+$)$_{20}$ dissolved in DMSO, (*D*) poly(**1-**^{t}**Bu**$^+$)$_{10}$-*b*-(**1-H**$^+$)$_{10}$ dissolved in DMSO, and (*E*) poly(**1-H**$^+$)$_{10}$-*r*-(**1-**^{t}**Bu**$^+$)$_{10}$ dissolved in DMSO. The polymer concentration tested (μg/mL) is provided along the outside edge of the petri dish. Control samples containing relevant solvent but no cationic polymers (indicated by a white box) were also tested and exhibited no ZOIs.

of bacterial inactivation, we note that some studies have shown that higher molar mass polymers with more cationic charges inactivate and disrupt bacterial cell membranes via surface contact (67–69). This is in contrast to other compounds that have to permeate into the cell membrane in order to inactivate the bacteria; in this case, higher molar mass polymers might exhibit poorer diffusion into the cell membrane, thus reducing their antibacterial efficacy (70).

Table 2. Comparison of the MIC, HC_{50}, and selectivity values of various homo- and copolymers

Sample	MIC (μg/mL)		HC_{50} (μg/mL)	Selectivity*	
	E. coli	MRSA		*E. coli*	MRSA
poly(**1**-H^+)$_{10}$	50	50	220	4.5	4.5
poly(**1**-H^+)$_{20}$	50	50	160	3.3	3.3
poly(**1**-H^+)$_{40}$	50	50	100	1.9	1.9
poly(**1**-^{t}**Bu**$^+$)$_{10}$	25	50	740	30	15
poly(**1**-^{t}**Bu**$^+$)$_{20}$	50	50	210	4.3	4.3
poly(**1**-^{t}**Bu**$^+$)$_{40}$	50	50	200	4.0	4.0
poly(**1**-^{t}**Bu**$^+$)$_{10}$-*b*-(**1**-H^+)$_{10}$	25	50	150	5.8	2.9
poly(**1**-H^+)$_{10}$-*r*-(**1**-^{t}**Bu**$^+$)$_{10}$	50	50	130	2.6	2.6

*Selectivity is calculated as HC_{50}/MIC.

Polymers with shorter chain length [DP = 10; poly(**1**$^+$)$_{10}$] and longer chain length [DP = 40; poly(**1**$^+$)$_{40}$] were compared to poly(**1**$^+$)$_{20}$ that was studied in the disk diffusion assays. An MIC value of 50 μg/mL against both *E. coli* and MRSA was measured for all tested poly(**1**-H^+) independent of their DP (Table 2). This MIC is markedly lower than the concentrations needed for bacterial inhibition in the disk diffusion assays. Notably, inconsistencies between disk diffusion and broth dilution evaluations have been reported and attributed to the ability of the polymer to diffuse from the filter disk and interact with bacteria-loaded, agar plate (71–73). To rule out a potential bactericidal effect of Ru impurities trapped in the polymer which are common in polymers synthesized via ROMP (74), the amount of residual Ru was measured by inductively coupled plasma mass spectrometry (ICP-MS). The Ru content was found to track with the initial feed ratios of monomer to catalyst and therefore to be higher in polymers with lower DPs (*SI Appendix*, Table S3). This finding suggests that Ru traces do not play a major role in the bioactivity of poly(**1**$^+$), which was found to be unaffected by changes in polymer length.

A similar study was conducted with *tert*-butyl substituted poly(**1**-^{t}**Bu**$^+$), as well as copolymers poly(**1**-^{t}**Bu**$^+$)$_{10}$-*b*-(**1**-H^+)$_{10}$ and poly(**1**-H^+)$_{10}$-*r*-(**1**-^{t}**Bu**$^+$)$_{10}$. However, because of the poor water solubility of these polymers, all samples were first dissolved in DMSO prior to dilution with Mueller Hinton Broth (MHB), which afforded MHB/polymer solutions with 5% DMSO content. Though high concentrations of organic solvents are generally incompatible with the growth of bacteria, low concentrations of DMSO (5%) are known not to inhibit the growth of *E. coli* or MRSA (71, 75). This was further confirmed by monitoring the bacterial growth curves of growth controls run with 5% DMSO in MHB (*SI Appendix*, Fig. S10 *E* and *F*). For this second series of cationic polymers, the broth microdilution assays were also found to be more sensitive to polymer concentrations than the disk diffusion assays. The MIC of poly(**1**-^{t}**Bu**$^+$)$_{20}$ and poly(**1**-^{t}**Bu**$^+$)$_{40}$ was 50 μg/mL for both bacteria (Table 2). Interestingly, the MIC of poly(**1**-^{t}**Bu**$^+$)$_{10}$ differed for *E. coli* (25 μg/mL) and MRSA (50 μg/mL). Similar to poly(**1**-^{t}**Bu**$^+$)$_{10}$, the block copolymer poly(**1**-^{t}**Bu**$^+$)$_{10}$-*b*-(**1**-H^+)$_{10}$ also resulted in MIC values of 25 and 50 μg/mL for *E. coli* and MRSA, respectively, whereas the random copolymer poly(**1**-H^+)$_{10}$-*r*-(**1**-^{t}**Bu**$^+$)$_{10}$ had an MIC value of 50 μg/mL for both bacteria. Differences in MIC values observed with Gram-negative and Gram-positive bacteria in the presence of antibacterial polymers are common and are typically ascribed to the specific outer membrane of each strain, which has been reported to impact the ability of bioactive compounds to diffuse into and/or interact with cellular membranes (70, 76, 77).

Cationic polymers with MIC values for *E. coli* or MRSA ranging from as low as 2 μg/mL to >1000 μg/mL (no activity) have been reported in the literature (4, 5, 78). The measured MIC values are therefore promising for the future implementation of structure–activity relationship studies owing to the modularity of the synthetic route and the livingness of the ROMP process. Additionally, highly bactericidal cationic polymers may poorly discriminate between mammalian and bacterial cells (26), which prompted us to investigate the hemolytic activity of poly(**1**-H^+) and poly(**1**-^{t}**Bu**$^+$).

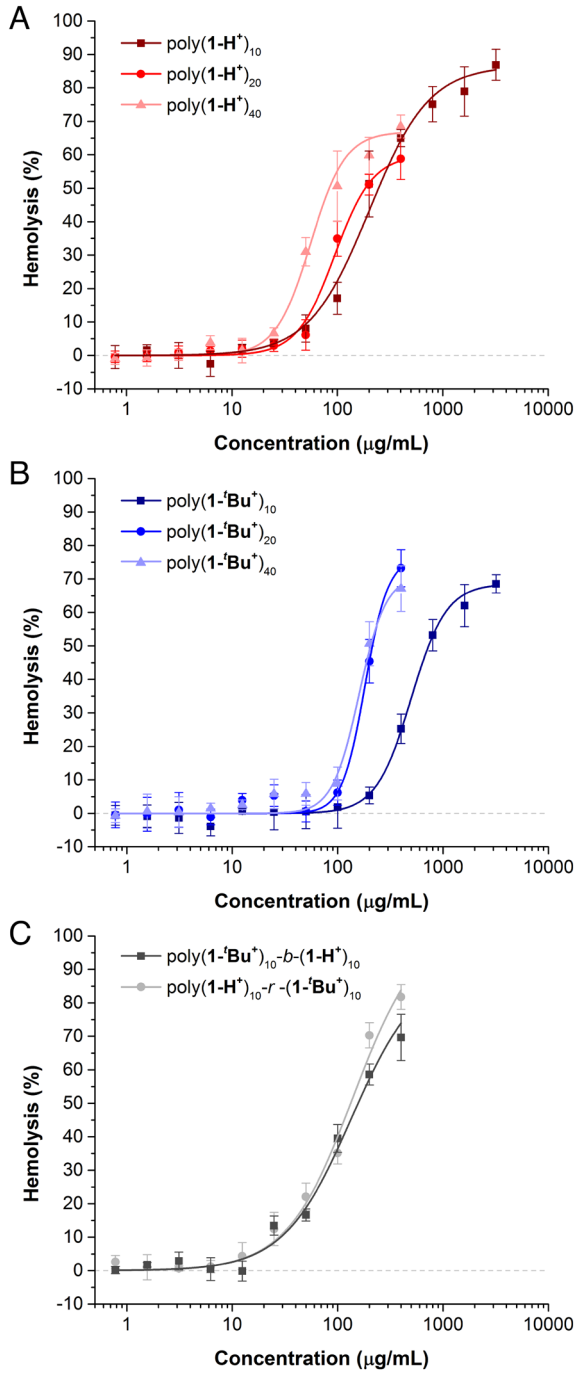

Fig. 7. Hemolytic activity of (*A*) poly(**1**-H^+), (*B*) poly(**1**-^{t}**Bu**$^+$), and (*C*) copolymers poly(**1**-^{t}**Bu**$^+$)$_{10}$-*b*-(**1**-H^+)$_{10}$ and poly(**1**-H^+)$_{10}$-*r*-(**1**-^{t}**Bu**$^+$)$_{10}$ against RBCs as a function of polymer concentration in RBC solution. Polymers of DP values of 20 or 40 were screened to maximum concentrations of 400 μg/mL due to their limited solubility in a majority phosphate-buffered saline (PBS) solution.

Determination of the Selectivity of Poly(1-H$^+$) and Poly(1-^{t}Bu$^+$) via Hemolysis Assays. A major structural factor impacting the antibacterial and hemolytic activities is the amphiphilicity of the polymer. Hydrophobic groups facilitate the insertion and disruption of a bacterial cell membrane, however excess hydrophobic motifs often lead to increased lysis of red blood cells (RBCs) (4). The hemolytic activity of all synthesized polymers against human RBCs was assessed through a hemoglobin release assay. The amount of hemolysis, H, was plotted as a function of polymer concentration for each synthesized macromolecule and fitted using Eq. **3** (Fig. 7):

$$H = \frac{1}{1 + \left(\frac{HC_{50}}{[P]}\right)^{n}}, \qquad [3]$$

where [P] is the polymer concentration, and HC_{50} (defined as the concentration of a polymer sample that results in 50% lysis of RBCs) and n are variable parameters. The HC_{50} value for each sample was calculated by fitting the data with Eq. **3**. The selectivity of poly(**1**-H$^+$) and poly(**1**-^{t}Bu$^+$) for bacterial cells over mammalian cells was subsequently determined using the ratio of HC_{50}/MIC (Table 2).

Unsubstituted poly(**1**-H$^+$) achieved a highest HC_{50} at a polymer concentration of 220 μg/mL for poly(**1**-H$^+$)$_{10}$ (Table 2). As the DP of poly(**1**-H$^+$) increased from a 10-mer to 20-mer and 40-mer, the HC_{50} values became significantly smaller. This suggests that, while the molar mass of poly(**1**-H$^+$) had little effect on antibacterial activity, it played a role on hemolytic activity, and therefore on the selectivity of the materials for bacterial cells. A similar trend was observed for poly(**1**-^{t}Bu$^+$), even though the *tert*-butyl substituted polymer had a significantly higher HC_{50} value for poly(**1**-^{t}Bu$^+$)$_{10}$ at 740 μg/mL. This sample resulted in the highest selectivity of poly(**1**-^{t}Bu$^+$) against both *E. coli* and MRSA. A *t* test confirmed that there was no significant difference in the hemolytic data from poly(**1**-^{t}Bu$^+$)$_{20}$ and poly(**1**-^{t}Bu$^+$)$_{40}$ [$t(18) = -0.080$, $P = 0.937$, *SI Appendix*]. Interestingly, the polymers with the lowest HC_{50} values (DP =10) contained the highest content of residual Ru (*SI Appendix*, Table S3). This observation aligns with our current hypothesis that Ru traces are not major contributors of the measured bioactivity of poly(**1**$^+$). Copolymers poly(**1**-^{t}Bu$^+$)$_{10}$-*b*-(**1**-H$^+$)$_{10}$ and poly(**1**-H$^+$)$_{10}$-*r*-(**1**-^{t}Bu$^+$)$_{10}$ that had a total DP of 20 cationic repeat units each were found to be both more toxic to RBCs than poly(**1**-H$^+$)$_{20}$ and poly(**1**-^{t}Bu$^+$)$_{20}$ homopolymers, with HC_{50} values of 150 and 130 μg/mL, respectively. Notably, no significant statistical differences between the hemolytic activities of the block and random copolymers were observed [$t(18) = 0.225$, $P = 0.824$]. Overall, the shortest cationic polymer of the more hydrophobic *tert*-butyl series, poly(**1**-^{t}Bu$^+$)$_{10}$, exhibited the best selectivity for both strains of bacteria (30 for *E. coli* and 15 for MRSA). This finding will guide the synthesis of polymers based on the pyridinium-fused polynorbornene scaffold with optimized bactericidal activity and selectivity.

Conclusion

In summary, we developed a controlled synthesis of main-chain cationic polymers via ROMP of pyridinium-fused norbornene monomers in EtOH using **Ru-3**. This precise process delivered macromolecules with tunable molar masses and cationic motifs independent of the media pH without the need of postpolymerization modifications. The resulting polymers, poly(**1**-H$^+$) and poly(**1**-^{t}Bu$^+$), demonstrated antibacterial activity against both Gram-negative *E. coli* and Gram-positive MRSA. Owing to the livingness of the optimized ROMP process, modification of the polymeric structure was performed through manipulation of the monomer-to-initiator ratio, random copolymerization, as well as synthesis of block copolymers via chain extension. In particular, the hydrophobicity around the cationic group was modulated through the addition of a lipophilic *tert*-butyl substituent on the pyridinium core. These modifications afforded MIC as low as 25 μg/mL against *E. coli* and 50 μg/mL against MRSA for poly(**1**-^{t}Bu$^+$)$_{10}$. Stark differences in hemolytic activities were measured across the pool of synthesized main-chain cationic polymers, which allowed the improvement of the selectivity value for bacterial cells over RBCs. In particular, shorter polymer chains (DP = 10) led to decreased hemolysis but maintained high bactericidal activity. Of note, the *N*-methylpyridinium-fused norbornene monomers did not inhibit bacterial growth, which demonstrated the importance of the polymeric architecture on the bioactivity. This study emphasizes the importance of complete structural control in the optimization of the bioactivity and selectivity of antibacterial polymers, including the location of the cations within the macromolecular structure (28).

Methods

See *SI Appendix* for the Materials, Analytical, Monomer Synthesis, Polymerization Screening Procedures, Kinetics Study, and Copolymer Synthesis subsections.

ROMP of 1$^+$ Catalyzed by Ru-3 Targeting Various DPs. In a nitrogen-filled glovebox, **Ru-3** was weighed into a 1-dram vial. The vial was hermetically sealed with a cap and electrical tape and then removed from the glovebox. Outside of the glovebox, EtOH (20 μL) was added to the vial to obtain a homogeneous solution of **Ru-3**. In a flame-dried 1-dram vial equipped with a stir bar was added monomer **1**-H$^+$ or **1**-^{t}Bu$^+$ (0.10 mmol) under nitrogen, followed by EtOH (100 μL). An aliquot of the **Ru-3** stock solution (10 μL, 1 equiv, see *SI Appendix*, Table S1 for specific amounts) was transferred to the solution of monomer **1**-H$^+$ or **1**-^{t}Bu$^+$ under nitrogen. The vial was then placed into a preheated oil bath at 60 °C, and the mixture was stirred for 3.5 h. Upon cooling to room temperature, ethyl vinyl ether (20 μL) was added, and the mixture was stirred for an additional 30 min. The crude mixture was diluted with d_4-MeOD (~1 mL), an aliquot (~200 μL) was removed and further diluted with d_4-MeOD (~400 μL). The diluted aliquot was used to determine monomer conversion via ^{1}H NMR spectroscopy. The polymer in the remaining solution was precipitated by addition of Et_2O, and the solid was isolated by centrifugation and decantation. The resulting material was dried under high vacuum at 70 °C. The material was then diluted to ~1.5 mg/mL with a solution of CF_3CO_2Na in TFE (C = 0.02 M) and analyzed by SEC.

Antibacterial Susceptibility Using Disk Diffusion Assays. Disk diffusion assays were conducted based on a previously published method (62) and Clinical and Laboratory Standard Institute (CLSI) guidelines (79). Whatman filter paper (Grade 3) was punched into 6 mm diameter disks using a hole puncher and sterilized via autoclave (80). Stock solutions of poly(**1**-H$^+$)$_{20}$ were made by dissolving the sample in either sterile DI water or DMSO, while stock solutions of poly(**1**-^{t}Bu$^+$)$_{20}$ were made by dissolving the sample in DMSO. Twofold serial dilutions were made by diluting the stock solution with its respective solvent. Test samples were prepared by pipetting 20 μL of a polymer dilution onto a filter disk, whereas the controls were loaded with 20 μL of solvent (no polymer). *E. coli* and MRSA were incubated in MHB at 37 °C with shaking (250 rpm) for 4 to 6 h until their logarithmic growth phase was reached in accordance with standards set by the CLSI. The liquid cultures of bacteria were diluted to an optical density (λ = 600 nm) of 0.1, which was approximately 10^8 CFU/mL and 10^7 CFU/mL, for *E. coli* and MRSA, respectively. Using a sterile cotton swab (Tifanso, Guangzhou, China), the bacterial suspension was streaked in three panes across the Mueller Hinton Agar plate (21 g/L MHB and 17 g/L agar in DI water autoclaved for 15 min at 120 °C). Agar plates were prepared using standard techniques and divided into six partitions for one control and five polymer dilutions (81). Inoculated disks were placed within each partition using flame-sterilized forceps. Agar plates containing samples were incubated for 16 h at 37 °C before the detection of a ZOI was used to determine the antibacterial susceptibility of a given polymer concentration.

MIC Determination by Microdilution Assays. Standardized broth microdilution protocols were followed for the needs of each of the different polymers (71, 81). For aqueous-soluble antibacterial agents–poly(**1-H**$^+$)–stock solutions were serial diluted with MHB in a 1:9 ratio before serial diluting the solutions twofold with MHB in 10 columns of a polypropylene 96-well plate. Each well contained a final volume of 50 μL of polymer solution. The bacteria suspension was diluted to a concentration of 10^6 CFU/mL before inoculating each well with 50 μL of bacteria. For non-aqueous-soluble antibacterial agents that require DMSO–poly(**1-^{t}Bu$^+$**), poly(**1-^{t}Bu$^+$**)-*b*-(**1-H$^+$**), and poly(**1-H$^+$**)-*r*-(**1-^{t}Bu$^+$**)–the polymers were dissolved in DMSO before diluting with MHB in a 1:9 ratio. In the well plate, stock solutions were serial diluted twofold in the first column with MHB followed by a serial twofold dilution with 5% DMSO in MHB in subsequent columns.

The last two columns of the well plate contained a growth control of bacteria inoculated in MHB and a sterile control of MHB without bacteria. The well plates were incubated (37 °C) in a BioTek Synergy HTX Multimode microplate reader for 16 h with continuous orbital shaking. The absorbance at $\lambda = 600$ nm was measured every 20 min. The MIC was determined as the lowest concentration that prevented the growth of bacteria.

Hemolysis Assays Using Human RBCs. Human RBCs were centrifuged (Eppendorf 5424 centrifuge) for 5 min at 1,500 rpm. The RBC pellet obtained was resuspended in PBS, and this procedure was repeated three times to remove the plasma and buffy coat. The 50% suspension of erythrocytes was diluted 20-fold in PBS to afford a 2.5% RBC suspension. All polymers were dissolved in DMSO at an initial concentration of 64,000 μg/mL, and each sample was serially diluted twofold to achieve the desired concentrations of polymer in DMSO.

Aliquots (10 μL) of each polymer dilution were added to a 96-well plate. To each well was added 90 μL of PBS and 100 μL of the 2.5% RBC suspension generating a total volume of 200 μL of a 1.25% suspension of cells with polymers at the desired concentration. The plates were incubated at 37 °C for 30 min. After the solutions from each well were centrifuged for 5 min at 1,500 rpm, 20 μL aliquots of the supernatants were transferred to a new 96-well plate and were diluted with 80 μL of PBS. The absorbance of hemoglobin present in the sample of each well was measured at 450 nm using a GlowMax-Multi+ plate reader. By incubating the RBC with 0.1% Triton X-100, 100% hemolysis data (positive control) were obtained. Background hemolysis (negative control) was evaluated by incubating the RBCs in 5% DMSO in PBS. All experiments were done in triplicate.

Hemolysis (H) for each sample was determined using Eq. **4**:

$$H(\%) = \left(\frac{OD_{450}(S) - OD_{450}(-)}{OD_{450}(+) - OD_{450}(-)} \right) \times 100 \qquad [4]$$

where $OD_{450}(S)$ is the optical density of the treated sample, $OD_{450}(-)$ is the optical density of the negative control, and $OD_{450}(+)$ is the optical density of the positive control. The data for the hemolysis assays are summarized in *SI Appendix*, Table S3. The hemolytic activity of monomers **1-H$^+$** and **1-^{t}Bu$^+$** was evaluated using the same protocol (*SI Appendix*, Fig. S11).

Data, Materials, and Software Availability. All study data are included in the article and/or *SI Appendix*.

ACKNOWLEDGMENTS. This work was supported by Texas A&M University and the NMR and Mass Spectrometry facilities in the Department of Chemistry were used, as well as the Texas A&M University Soft Matter Facility (RRID:SCR_022482). This work was supported by the National Institute of General Medical Sciences at the NIH under Award Number R35GM138079. We thank Dr. Mara Kuenen and Dr. Rachel Letteri (University of Virginia) for their assistance with SEC analysis; Dr. Lauren Andrews (University of Massachusetts Amherst) and Dr. Robin Patel (Mayo Clinic) for their kind donations of bacteria; and Nathan Williams and Dr. Jean-Philippe Pellois (Texas A&M University) for their technical assistance with hemolysis assays. E.D. acknowledges support from the Spaulding Smith Fellowship.

Author affiliations: [a]Department of Chemistry, Texas A&M University, College Station, TX 77843; [b]Department of Chemical Engineering, University of Massachusetts, Amherst, MA 01003; and [c]Department of Materials Science and Engineering, Texas A&M University, College Station, TX 77843

Author contributions: S.N.H., N.Y., E.D., J.D.S., and Q.M. designed research; S.N.H., N.Y., E.D., A.M., and A.T. performed research; S.N.H., N.Y., E.D., A.M., A.T., J.D.S., and Q.M. analyzed data; and S.N.H., E.D., J.D.S., and Q.M. wrote the paper.

1. G. Sun *et al.*, Antibiotic resistant bacteria: A bibliometric review of literature. *Front. Public Health* **10**, 1002015 (2022), 10.3389/fpubh.2022.1002015.
2. K. Lewis, Platforms for antibiotic discovery. *Nat. Rev. Drug Discovery* **12**, 371–387 (2013).
3. World Health Organization, Antibiotic resistance. WHO. https://www.who.int/news-room/fact-sheets/detail/antibiotic-resistance. Accessed 28 November 2023.
4. M. S. Ganewatta, C. Tang, Controlling macromolecular structures towards effective antimicrobial polymers. *Polymer* **63**, A1–A29 (2015).
5. Y. Yang, Z. Cai, Z. Huang, X. Tang, X. Zhang, Antimicrobial cationic polymers: From structural design to functional control. *Polym. J.* **50**, 33–44 (2018).
6. C. Ergene, K. Yasuhara, E. F. Palermo, Biomimetic antimicrobial polymers: Recent advances in molecular design. *Polym. Chem.* **9**, 2407–2427 (2018).
7. H. Luo *et al.*, Polymeric antibacterial materials: Design, platforms and applications. *J. Mater. Chem. B* **9**, 2802–2815 (2021).
8. Z. Si *et al.*, Polymers as advanced antibacterial and antibiofilm agents for direct and combination therapies. *Chem. Sci.* **13**, 345–364 (2022).
9. P. Pham, S. Oliver, C. Boyer, Design of antimicrobial polymers. *Macromol. Chem. Phys.* **224**, 2200226 (2023).
10. I. Sovadinová, K. Kuroda, E. F. Palermo, Unexpected enhancement of antimicrobial polymer activity against Staphylococcus aureus in the presence of fetal bovine serum. *Molecules* **26**, 4512 (2021).
11. L. T. Nguyen, E. F. Haney, H. J. Vogel, The expanding scope of antimicrobial peptide structures and their modes of action. *Trends Biotechnol.* **29**, 464–472 (2011).
12. P. Gilbert, L. E. Moore, Cationic antiseptics: Diversity of action under a common epithet. *J. Appl. Microbiol.* **99**, 703–715 (2005).
13. L. Yu *et al.*, Antimicrobial peptides and macromolecules for combating microbial infections: From agents to interfaces. *ACS Appl. Bio Mater.* **5**, 366–393 (2022).
14. N. Mookherjee, M. A. Anderson, H. P. Haagsman, D. J. Davidson, Antimicrobial host defence peptides: Functions and clinical potential. *Nat. Rev. Drug Discov.* **19**, 311–332 (2020).
15. A. Kuroki *et al.*, Sequence control as a powerful tool for improving the selectivity of antimicrobial polymers. *ACS Appl. Mater. Interfaces* **9**, 40117–40126 (2017).
16. P. T. Phuong *et al.*, Effect of hydrophobic groups on antimicrobial and hemolytic activity: Developing a predictive tool for ternary antimicrobial polymers. *Biomacromolecules* **21**, 5241–5255 (2020).
17. A. Kanazawa, T. Ikeda, T. Endo, Antibacterial activity of polymeric sulfonium salts. *J. Polym. Sci. Part A Polym. Chem.* **31**, 2873–2876 (1993).
18. E. F. Palermo, K. Kuroda, Chemical structure of cationic groups in amphiphilic polymethacrylates modulates the antimicrobial and hemolytic activities. *Biomacromolecules* **10**, 1416–1428 (2009).
19. E. F. Palermo, S. Vemparala, K. Kuroda, Cationic spacer arm design strategy for control of antimicrobial activity and conformation of amphiphilic methacrylate random copolymers. *Biomacromolecules* **13**, 1632–1641 (2012).
20. A. Punia, A. Mancuso, P. Banerjee, N.-L. Yang, Nonhemolytic and antibacterial acrylic copolymers with hexamethyleneamine and poly(ethylene glycol) side chains. *ACS Macro Lett.* **4**, 426–430 (2015).
21. J. L. Grace *et al.*, Cationic acrylate oligomers comprising amino acid mimic moieties demonstrate improved antibacterial killing efficiency. *J. Mater. Chem. B* **5**, 531–536 (2017).
22. G. J. Gabriel *et al.*, Synthetic mimic of antimicrobial peptide with nonmembrane-disrupting antibacterial properties. *Biomacromolecules* **9**, 2980–2983 (2008).
23. A. P. Kaymaz *et al.*, Synthesis of 1,4-diazabicyclo[2.2.2]octane and pyridinium based cationic polymers via ROMP technique and examination of their antibacterial activity and cytotoxicity. *Materialia* **5**, 100246 (2019).
24. K. Lienkamp *et al.*, Antimicrobial polymers prepared by ROMP with unprecedented selectivity: A molecular construction kit approach. *J. Am. Chem. Soc.* **130**, 9836–9843 (2008).
25. K. Lienkamp, A. E. Madkour, K.-N. Kumar, K. Nüsslein, G. N. Tew, Antimicrobial polymers prepared by ring-opening metathesis polymerization: Manipulating antimicrobial properties by organic counterion and charge density variation. *Chem. – Eur. J.* **15**, 11715–11722 (2009).
26. Y. Lou, J. Gaitor, M. Treichel, K. J. T. Noonan, E. F. Palermo, Biocidal potency of polymers with bulky cations. *ACS Macro Lett.* **12**, 215–220 (2023).
27. J. Guo *et al.*, Antibacterial activity of cationic polymers: Side-chain or main-chain type? *Polym. Chem.* **9**, 4611–4616 (2018).
28. S. Laroque *et al.*, Synthetic star nanoengineered antimicrobial polymers as antibiofilm agents: Bacterial membrane disruption and cell aggregation. *Biomacromolecules* **24**, 3073–3085 (2023).
29. Y. Hu, J. Zhao, J. Zhang, Z. Zhu, J. Rao, Broad-spectrum bactericidal activity and remarkable selectivity of main-chain sulfonium-containing polymers with alternating sequences. *ACS Macro Lett.* **10**, 990–995 (2021).
30. J. Oh, A. Khan, Main-chain polysulfonium salts: Development of non-ammonium antibacterial polymers similar in their activity to antibiotic drugs vancomycin and kanamycin. *Biomacromolecules* **22**, 3534–3542 (2021).
31. X. Wang, G. Wang, J. Zhao, Z. Zhu, J. Rao, Main-chain sulfonium-containing homopolymers with negligible hemolytic toxicity for eradication of bacterial and fungal biofilms. *ACS Macro Lett.* **10**, 1643–1649 (2021).
32. J. Zhao, Z. Zhu, J. Rao, Development of cationic sulfonium-based gels with inherent antibacterial, excellent antibiofilm, and tunable swelling properties. *Eur. Polym. J.* **179**, 111551 (2022).
33. Y. Zhao *et al.*, Enhanced synergistic antibacterial and antibiofilm efficacy of main-chain polysulfoniums with antibiotics by balancing charge density and amphiphilicity. *ACS Appl. Polym. Mater.* **5**, 4437–4447 (2023).
34. M. C. Stuparu, A. Khan, Poly(ß-hydroxy thioether)s: Synthesis through thiol-epoxy 'click' reaction and post-polymerization modification to main-chain polysulfonium salts. *J. Macromol. Sci. Part A* **59**, 2–10 (2022).
35. R. J. Kopiasz *et al.*, Influence of PEG subunit on the biological activity of ionenes: Synthesis of novel polycations, antimicrobial and toxicity studies. *Macromol. Biosci.* **22**, 2200094 (2022).

36. R. J. Kopiasz *et al.*, Hydrophilic quaternary ammonium ionenes–is there an influence of backbone flexibility and topology on antibacterial properties? *Macromol. Biosci.* **20**, 2000063 (2020).
37. S. Liu *et al.*, Highly potent antimicrobial polyionenes with rapid killing kinetics, skin biocompatibility and in vivo bactericidal activity. *Biomaterials* **127**, 36–48 (2017).
38. C. Mattheis, M. Zheng, S. Agarwal, Closing one of the last gaps in polyionene compositions: Alkyloxyethylammonium ionenes as fast-acting biocides. *Macromol. Biosci.* **12**, 341–349 (2012).
39. L. Liu *et al.*, Main-chain imidazolium oligomer material as a selective biomimetic antimicrobial agent. *Biomaterials* **33**, 8625–8631 (2012).
40. X. Xu *et al.*, A novel comb-like ionenes with aliphatic side chains: Synthesis and antimicrobial properties. *J. Mater. Sci.* **48**, 1162–1171 (2013).
41. A. Pascual *et al.*, Broad-spectrum antimicrobial polycarbonate hydrogels with fast degradability. *Biomacromolecules* **16**, 1169–1178 (2015).
42. Y. Yuan, S. Liang, J. Li, S. Zhang, Y. Zhang, Copolymers with both soft and rigid cationic rings as highly selective antimicrobials to combat antibiotic resistant microbes and biofilms. *J. Mater. Chem. B* **7**, 5620–5625 (2019).
43. Y. Qiao *et al.*, Highly dynamic biodegradable micelles capable of lysing Gram-positive and Gram-negative bacterial membrane. *Biomaterials* **33**, 1146–1153 (2012).
44. K. E. S. Locock *et al.*, Guanylated polymethacrylates: A class of potent antimicrobial polymers with low hemolytic activity. *Biomacromolecules* **14**, 4021–4031 (2013).
45. K. Lienkamp, K.-N. Kumar, A. Som, K. Nüsslein, G. N. Tew, "Doubly selective" antimicrobial polymers: How do they differentiate between bacteria? *Chem. – Eur. J.* **15**, 11710–11714 (2009).
46. W. Chin *et al.*, Biodegradable broad-spectrum antimicrobial polycarbonates: Investigating the role of chemical structure on activity and selectivity. *Macromolecules* **46**, 8797–8807 (2013).
47. K. Kuroda, W. F. DeGrado, Amphiphilic polymethacrylate derivatives as antimicrobial agents. *J. Am. Chem. Soc.* **127**, 4128–4129 (2005).
48. A. Strassburg *et al.*, Nontoxic, hydrophilic cationic polymers–identified as class of antimicrobial polymers. *Macromol. Biosci.* **15**, 1710–1723 (2015).
49. FDA, Drug Products, *Including Biological Products, that Contain Nanoparticles; Guidance for Industry* (U.S. Food and Drug Administration, 2022).
50. W. You, K. J. T. Noonan, G. W. Coates, Alkaline-stable anion exchange membranes: A review of synthetic approaches. *Prog. Polym. Sci.* **100**, 101177 (2020).
51. T. J. Clark *et al.*, A ring-opening metathesis polymerization route to alkaline anion exchange membranes: Development of hydroxide-conducting thin films from an ammonium-functionalized monomer. *J. Am. Chem. Soc.* **131**, 12888–12889 (2009).
52. C. Wang *et al.*, Crosslinked norbornene copolymer anion exchange membrane for fuel cells. *J. Membr. Sci.* **556**, 118–125 (2018).
53. W. You, K. M. Hugar, G. W. Coates, Synthesis of alkaline anion exchange membranes with chemically stable imidazolium cations: Unexpected cross-linked macrocycles from ring-fused romp monomers. *Macromolecules* **51**, 3212–3218 (2018).
54. W. You, E. Padgett, S. N. MacMillan, D. A. Muller, G. W. Coates, Highly conductive and chemically stable alkaline anion exchange membranes via ROMP of trans-cyclooctene derivatives. *Proc. Natl. Acad. Sci. U.S.A.* **116**, 9729–9734 (2019).
55. C. T. Womble, G. W. Coates, K. Matyjaszewski, K. J. T. Noonan, Tetrakis(dialkylamino)phosphonium polyelectrolytes prepared by reversible addition-fragmentation chain transfer polymerization. *ACS Macro Lett.* **5**, 253–257 (2016).
56. L. Gu, H. Dong, Z. Sun, Y. Li, F. Yan, Spirocyclic quaternary ammonium cations for alkaline anion exchange membrane applications: An experimental and theoretical study. *RSC Adv.* **6**, 94387–94398 (2016).
57. S. N. Hancock, N. Yuntawattana, S. M. Valdez, Q. Michaudel, Expedient synthesis and ring-opening metathesis polymerization of pyridinonorbornenes. *Polym. Chem.* **13**, 5530–5535 (2022).
58. D. A. Rankin, S. J. P'Pool, H.-J. Schanz, A. B. Lowe, The controlled homogeneous organic solution polymerization of new hydrophilic cationic exo–7–oxanorbornenes via ROMP with RuCl2(PCy3)2CHPh in a novel 2,2,2-trifluoroethanol/methylenechloride solvent mixture. *J. Polym. Sci. Part A Polym. Chem.* **45**, 2113–2128 (2007).
59. K. Skowerski *et al.*, Highly active catalysts for olefin metathesis in water. *Catal. Sci. Technol.* **2**, 2424–2427 (2012).
60. B. S. Aitken, M. Lee, M. T. Hunley, H. W. Gibson, K. B. Wagener, Synthesis of precision ionic polyolefins derived from ionic liquids. *Macromolecules* **43**, 1699–1701 (2010).
61. K. O. Kim, S. Shin, J. Kim, T.-L. Choi, Living polymerization of monomers containing endo-tricyclo [4.2.2.02,5]deca-3,9-diene using second generation Grubbs and Hoveyda-Grubbs catalysts: approach to synthesis of well-defined star polymers. *Macromolecules* **47**, 1351–1359 (2014).
62. A. W. Bauer, W. M. M. Kirby, J. C. Sherris, M. Turck, Antibiotic susceptibility testing by a standardized single disk method. *Am. J. Clin. Pathol.* **45**, 493–496 (1966).
63. M. Balouiri, M. Sadiki, S. K. Ibnsouda, Methods for in vitro evaluating antimicrobial activity: A review. *J. Pharm. Anal.* **6**, 71–79 (2016).
64. P. C. Kohner, J. E. Rosenblatt, F. R. Cockerill, Comparison of agar dilution, broth dilution, and disk diffusion testing of ampicillin against Haemophilus species by using in-house and commercially prepared media. *J. Clin. Microbiol.* **32**, 1594–1596 (1994).
65. D. Liu, Y. K. Chau, B. J. Dutka, Rapid toxicity assessment of water-soluble and water-insoluble chemicals using a modified agar plate method. *Water Res.* **23**, 333–339 (1989).
66. R. C. Brito, G. N. Silva, T. C. Farias, P. B. Ferreira, S. B. Ferreira, Standardization of the safety level of the use of DMSO in viability assays in bacterial cells. *MOL2NET* **3**, 1–6 (2017).
67. A. Tyagi, A. Mishra, Optimal balance of hydrophobic content and degree of polymerization results in a potent membrane-targeting antibacterial polymer. *ACS Omega* **6**, 34724–34735 (2021).
68. W. Zhong, Y. Chang, Y. Lin, A. Zhang, Synthesis and antifungal activities of hydrophilic cationic polymers against Rhizoctonia solani. *Fungal Biol.* **124**, 735–741 (2020).
69. T. D. Michl *et al.*, Bacterial membrane permeability of antimicrobial polymethacrylates: Evidence for a complex mechanism from super-resolution fluorescence imaging. *Acta Biomater.* **108**, 168–177 (2020).
70. D. Trombetta *et al.*, Mechanisms of antibacterial action of three monoterpenes. *Antimicrob. Agents Chemother.* **49**, 2474–2478 (2005).
71. S. Alharthi, Z. M. Ziora, P. M. Moyle, Optimized protocols for assessing libraries of poorly soluble sortase A inhibitors for antibacterial activity against medically-relevant bacteria, toxicity and enzyme inhibition. *Biorg. Med. Chem.* **52**, 116527 (2021).
72. A. Klančnik, S. Piskernik, B. Jeršek, S. S. Možina, Evaluation of diffusion and dilution methods to determine the antibacterial activity of plant extracts. *J. Microbiol. Methods* **81**, 121–126 (2010).
73. F. Hadacek, H. Greger, Testing of antifungal natural products: Methodologies, comparability of results and assay choice. *Phytochem. Anal.* **11**, 137–147 (2000).
74. C. Kim, B. A. Ondrusek, H. Chung, Removable water-soluble olefin metathesis catalyst via host-guest interaction. *Org. Lett.* **20**, 736–739 (2018).
75. H. Mi *et al.*, Dimethyl sulfoxide protects *Escherichia coli* from rapid antimicrobial-mediated killing. *Antimicrob. Agents Chemother.* **60**, 5054–5058 (2016).
76. I. M. Helander *et al.*, Characterization of the action of selected essential oil components on gram-negative bacteria. *J. Agric. Food. Chem.* **46**, 3590–3595 (1998).
77. R. E. W. Hancock, The bacterial outer membrane as a drug barrier. *Trends Microbiol.* **5**, 37–42 (1997).
78. M. Venkatesh *et al.*, Activity and cell selectivity of synthetic and biosynthetic cationic polymers. *Antimicrob. Agents Chemother.* **61**, e00469-17 (2017).
79. CLSI, *Methods for Determining Bactiericidal Activity of Antimicrobial Agents; Approved Guideline* (CLSI document M26-A. Wayne, PA, USA: Clinical and Laboratory Standards Institute, 1999).
80. N. Vineetha, R. A. Vignesh, D. Sridhar, Preparation, standardization of antibiotic discs and study of resistance pattern for first-line antibiotics in isolates from clinical samples. *Int. J. Appl. Res.* **1**, 624–631 (2015).
81. I. Wiegand, K. Hilpert, R. E. W. Hancock, Agar and broth dilution methods to determine the minimal inhibitory concentration (MIC) of antimicrobial substances. *Nat. Protoc.* **3**, 163–175 (2008).